Journal of Hazardous Materials 192 (2011) 1002–1008

Contents lists available at ScienceDirect

Journal of Hazardous Materials

journal homepage: www.elsevier.com/locate/jhazmat

High efficiency removal of dissolved As(III) using iron nanoparticle-embedded macroporous polymer composites

Irina N. Savina[a,b,*], Christopher J. English[a], Raymond L.D. Whitby[a], Yishan Zheng[b], Andre Leistner[c], Sergey V. Mikhalovsky[b], Andrew B. Cundy[a]

[a] Nanoscience & Nanotechnology Group, Faculty of Science & Engineering, University of Brighton, Lewes Road, Brighton BN2 4GJ, UK
[b] Biomaterials Group, Faculty of Science & Engineering, University of Brighton, Lewes Road, Brighton BN2 4GJ, UK
[c] Polymerics GmbH, Landsberger Allee 378A, 12681 Berlin, Germany

ARTICLE INFO

Article history:
Received 26 January 2011
Received in revised form 19 May 2011
Accepted 2 June 2011
Available online 12 June 2011

Key words:
Water remediation
Adsorbent
Arsenic
Iron
Nanoparticle

ABSTRACT

Novel nanocomposite materials where iron nanoparticles are embedded into the walls of a macroporous polymer were produced and their efficiency for the removal of As(III) from aqueous media was studied. Nanocomposite gels containing α-Fe_2O_3 and Fe_3O_4 nanoparticles were prepared by cryopolymerisation resulting in a monolithic structure with large interconnected pores up to 100 μm in diameter and possessing a high permeability (*ca.* 3×10^{-3} m s^{-1}). The nanocomposite devices showed excellent capability for the removal of trace concentrations of As(III) from solution, with a total capacity of up to 3 mg As/g of nanoparticles. The leaching of iron was minimal and the device could operate in a pH range 3–9 without diminishing removal efficiency. The effect of competing ions such as SO_4^{2-} and PO_4^{3-} was negligible. The macroporous composites can be easily configured into a variety of shapes and structures and the polymer matrix can be selected from a variety of monomers, offering high potential as flexible metal cation remediation devices.

1. Introduction

Nanoscale particles have a large surface area, available for interaction with contaminants, high surface reactivity and could provide cost effective solutions to many challenging environmental remediation problems [1]. For example, zero valent iron nanoparticles of a diameter 1–100 nm and with a surface area in the range 20–40 m^2/g, provide 10–1000 times greater reactivity than granular iron, which has a surface area <1 m^2/g [2]. Decreasing Fe_3O_4 particle size from 300 nm to 12 nm was shown to increase their adsorption capacity for As(III) and As(V) 200 fold [3].

Iron nanoparticles have been shown to be effective in the transformation, detoxification and/or sorption of a wide variety of common environmental contaminants, such as chlorinated organic solvents, organochlorine pesticides, and polychlorinated biphenyls [1,4], heavy metals and metalloids (As(III), Pb(II), Cu(II), Ni(II), Cr(VI)) and radionuclides [5], in both *ex situ* and *in situ* (e.g. via direct injection to subsurface environments) applications [6]. While the high reactivity and often high environmental mobility of nanoparticles offer a number of advantages over conventional environmental remediation technologies, there are however a number of potentially serious issues concerning the environmental fate of engineered nanoparticles and their potential impact on human health [7]. Because of their small size, nanoparticles can enter the body via dermal routes, by ingestion or inhalation. The toxicity of nanoparticles has been studied by numerous authors who have raised concerns of the potentially adverse effects of such engineered or industrially manufactured systems resulting from their production and large scale application [8,9]. A range of ecotoxicological effects from manufactured nanoparticles have been reported on microbes, plants, invertebrates and fish species, as well as mammals [8–10]. In particular, the potentially adverse effects of iron nanoparticle uptake, such as oxidative stress response, DNA and protein damage, mutagenic effects and cell death, have been reported by a number of workers [11,12]. In general, the transport mechanisms of engineered nanoparticles through the environment and into plants and animals, and the associated risks, remain poorly understood [13] and this may significantly limit their widespread application as remediation materials, particularly where methods involve free-release of engineered nanoparticles to the environment.

Immobilizing nanoparticles onto a bulk carrier can, however, prevent their release into the environment while maintaining their reactivity. A number of water remediation devices have been developed based on iron nanoparticles immobilized into polymer matrices, which are usually produced as beads or fibres [14–16].

* Corresponding author. Tel.: +44 1273 642015; fax: +44 1273 642674.
E-mail address: i.n.savina@brighton.ac.uk (I.N. Savina).

0304-3894/$ – see front matter © 2011 Elsevier B.V. All rights reserved.
doi:10.1016/j.jhazmat.2011.06.003

In particular, iron oxide nanoparticles immobilized in a gel bead matrix (under the trade names 'ArsenX^{np}' and 'npRio') are commercially available and have been used successfully in filter bed or column flow-through formats [17]. The use of beads however, imposes limitations on the configuration and wider environmental/industrial application of these devices. Here, we examine the properties of novel macroporous iron nanoparticle–polymer composite monoliths, produced by cryopolymerisation, and assess their potential application in water remediation, particularly for removal of the important groundwater contaminant As(III).

2. Materials and methods

2.1. Materials

2-Hydroxyethyl methacrylate (HEMA, 98%) was sourced from Acros Organics (Geel, Belgium). Poly(ethylene glycol)diacrylate (PEGDA, $M_n \sim 258$) was obtained from Aldrich (Steinheim, Germany). Ammonium persulfate (APS, 98%) and N,N,N′,N′-tetramethylethylenediamine (TEMED, 99%) were from Thermo Scientific (Rockford, USA). Iron nanoparticles α-Fe_2O_3 and Fe_3O_4 were obtained from Arry International Group Limited (Köln, Germany). Average particle size was 30 nm and 20 nm for α-Fe_2O_3 and Fe_3O_4, respectively. As(III) oxide was obtained from Argos Chemicals (NJ, USA). Silica-based strong anion-exchange (SAX) cartridges containing 500 mg sorbent of 40-μm particle size and 60-Å pore size were obtained from Supelco (Bellefonte, USA).

2.2. Methods

2.2.1. Macroporous iron nanoparticle-polymer monolith preparation

Monolithic macroporous composite gels were prepared by the polymerization of HEMA and PEGDA. Iron particles were mixed with a monomer solution of HEMA (5.8% v/v) and PEGDA (1.8% v/v). The reaction mixture was placed in an ultrasonic bath for 30 min and then cooled in an ice bath for 10 min. The reaction mixture was shaken again to obtain a homogeneous distribution of the nanoparticles, and then TEMED/APS (1.2 w/w % of monomer) were added. One milliliter of the reaction solution was quickly added into separate glass tubes (80 mm × 11 mm i.d.) that were closed at the bottom with a silicon cap. The solution in the tubes was frozen in a Julabo cooling chamber at −12 or −18 °C, incubated at that temperature for 18 h and then thawed at room temperature. The caps were removed and gels were washed by passing 50 ml of deionised water through each sample.

2.2.2. Permeability measurements

The flow rate of liquid passing through the column was measured at a constant hydrostatic pressure equal to a 100 cm head of water-column, which corresponds to a pressure of *ca.* 0.01 MPa on the cryogel composite [18].

2.2.3. Mechanical properties

Mechanical properties of the composite gel were tested using a dynamic mechanical analyzer (DMA 2980 TA Instruments, Inc., USA) with a cell load of 0.01 N. The gel samples (cylinders of 10 mm height and diameter of 10 mm) were placed between two plates and compressed with a steadily increasing pressure of 5 N/min to the maximum loading 18 N. All samples were tested at room temperature. Compression modulus and stiffness were obtained from the stress-strain curve. The stiffness was estimated as the stress, in MPa, necessary to achieve an 80% compression.

2.2.4. Iron content measurement

Iron content was measured by extraction of iron with 2 M HCl solution. Composite gel pieces (70–100 mg) were incubated in 10 ml of 2 M HCl. The solution was removed from the composite gel regularly for concentration measurements and replaced with fresh 2 M HCl solution. Iron concentration in solution was measured using a Perkin Elmer Optima^{TM} 2100 DV ICP-OES system. The procedure was repeated until no iron was detected in the extract. Around 70–90% of iron was extracted in the first 3 days. Total iron extraction was continued for 38 days. Additionally, iron particle content was estimated by thermogravimetric analysis (TGA). The composite gel was dried at 80 °C for 2 days. The TGA profile was recorded from 50 °C to 800 °C at a scanning rate of 10 °C/min. TGA analysis of the top, middle and bottom sections of the composite gel monolith was performed and average results are presented in Table 1.

2.2.5. Scanning electron microscopy (SEM)

Samples for scanning electron microscopy were prepared by freeze-drying the composite gels overnight. After drying, specimens were mounted on aluminium stubs fitted with adhesive carbon pads, sputter coated with palladium and examined using a JEOL JSM-6310 scanning electron microscope.

2.2.6. Transmission electron microscopy (TEM)

The gel samples were dehydrated by washing with ethanol water mixtures with increasing ethanol concentration of 10, 20, 30, 50 and 75% ethanol for 20 min each and dried in absolute ethanol. Ethanol was replaced with propylene oxide, which then was replaced with TAAB low viscosity resin (TAAB Laboratories Equipment Ltd, UK). After complete replacement, the resin was polymerized at 60 °C. Thin (100 nm) sections were cut on a Leica Ultracut ultramicrotome, collected on nickel support grids and examined unstained with a Hitachi-7100 TEM at 100 kV. Images were acquired digitally with an axially mounted (2k × 2k pixel) Gatan Ultrascan 1000 CCD camera (Gatan UK, Oxford, UK).

2.2.7. As(III) solution preparation

A stock solution of As(III) was prepared as follows. Powdered arsenious oxide (2.5 g, As_4O_6) was dissolved in sodium hydroxide solution (2 g in 20 ml of deionised water). The volume was adjusted with deionised water to 200 ml. The pH of the solution was adjusted to 6.5 and 2 g of sodium bicarbonate was added. Finally the volume of solution was made up to 500 ml. The stock solution was then used throughout all experiments for preparation of arsenic (III) solution of varying dilutions.

2.2.8. Measuring the arsenic speciation in the solution.

Arsenic speciation was determined according to a previously published procedure [19]. A volume of 10 ml of As(III) solution was passed through a SAX cartridge at a flow rate 0.5 ml/min. Cartridges were preconditioned with 50% ethanol and deionised water prior to use. Then 10 ml of deionised water was passed through, and finally 15 ml of 1.0 M HCl was pumped at a flow rate 0.5 ml/min. Fractions of 5 ml were collected and As(III) concentration before and after adsorption was measured using a Perkin Elmer Optima^{TM} 2100 DV ICP-OES system (detection limit 5 ppb, according to Perkin Elmer specification).

2.2.9. Assessing the adsorption capacity of iron nanoparticles and nanocomposite gels

The gel (0.5 ml) was cut into small cubic pieces of 2 mm in size. 10, 30 or 100 ml of As(III) solution (2 mg/l) were added, and the samples were shaken for 24 h at room temperature. Iron oxide nanoparticles (20, 60 and 80 mg) were weighed in centrifuge tubes,

Table 1
Properties of composite gels.

Gel	Flow rate ($m\,s^{-1}$)	Particle concentration, determined:			
		by extraction with 2 M HCl		by TGA analysis	
		g/g hydrated gel	g/g dried gel	g/g hydrated gel	g/g dried gel
HEMA–MG (HEMA cryogel, without particles)	$(2.47 \pm 0.5) \times 10^{-3}$	0	0	0	0
α-Fe_2O_3–MG	$(2.29 \pm 0.34) \times 10^{-3}$	0.059	0.37	0.077	0.48
Fe_3O_4–MG	$(2.78 \pm 0.33) \times 10^{-3}$	0.095	0.59	0.078	0.49

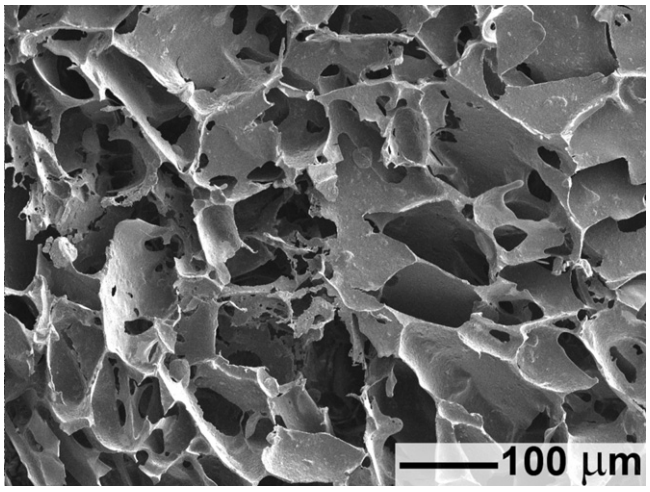

Fig. 1. SEM image of composite Fe_3O_4–MG, revealing the interconnected macropores separated by thin polymer walls. Gels were prepared at −12 °C.

then 20 or 40 ml of As(III) solution (4 mg/l) were added and the samples were shaken for 24 h at room temperature. Nanoparticles were separated from the solution by centrifugation. From each sample 5 ml aliquots were taken for measuring arsenic concentration. The maximum adsorption capacity for nanoparticles and nanocomposites is presented in Table 3. Arsenic concentrations before and after adsorption were measured using a Perkin Elmer Optima™ 2100 DV ICP-OES system.

2.2.10. pH effect

The composite gel was cut into small pieces of 2 mm size. Ten ml of 5 mg/l As(III) solution was added to 0.5 g of gel and samples were put on a shaking table for 1.5 h and 3 h with α-Fe_2O_3–gel and Fe_3O_4–gel, respectively. The pH of As(III) solution was adjusted with HCl and NaOH and was in the range between 3.0 and 12. Aliquots of 3 ml were withdrawn and measured using a Perkin Elmer Optima™ 2100 DV ICP-OES system.

2.2.11. Effect of PO_4^{3-} and SO_4^{2-} on As(III) adsorption for α-Fe_2O_3 and Fe_3O_4 composite gel

The composite gel was cut into small pieces of 2 mm size. Twenty milliliter of 5 mg/l As(III) solution with different content of PO_4^{3-} or SO_4^{2-} was added to 0.4 g of gel and samples were put on a shaking table for 20 h. The pH of solutions containing PO_4^{3-} was adjusted to 7.0 with HCl. Aliquots of 3 ml were withdrawn and measured using a Perkin Elmer Optima™ 2100 DV ICP-OES system.

2.2.12. Kinetics of As(III) adsorption

The composite gel was cut into small pieces of 2 mm size. As(III) solution (500 ml, 2 mg/l, pH 7.0) was added to 4.5 ml of gel with vigorous stirring. Samples of 2 ml were periodically withdrawn and As(III) concentrations were measured using a Perkin Elmer Optima™ 2100 DV ICP-OES system.

3. Results and discussion

3.1. Cryopolymers

Cryogelation is a versatile technique allowing the preparation of mechanically robust polymer gels, possessing large interconnected pores of up to 100 μm diameter, with high permeability and very low flow resistance when used in a column configuration [20–23]. The method is based on gel formation at a temperature below the freezing point of the solvent. When water, a common solvent for gel formation, freezes out, the ice crystals formed expel the monomers, cross-linker and initiator, which concentrate into the unfrozen liquid phase which can be supercooled even at −20 °C. Gels are formed in the unfrozen liquid phase generating a dense, highly cross-linked polymer. After melting the ice crystals large voids remain, creating a continuous system of channels – an interconnected pore sys-

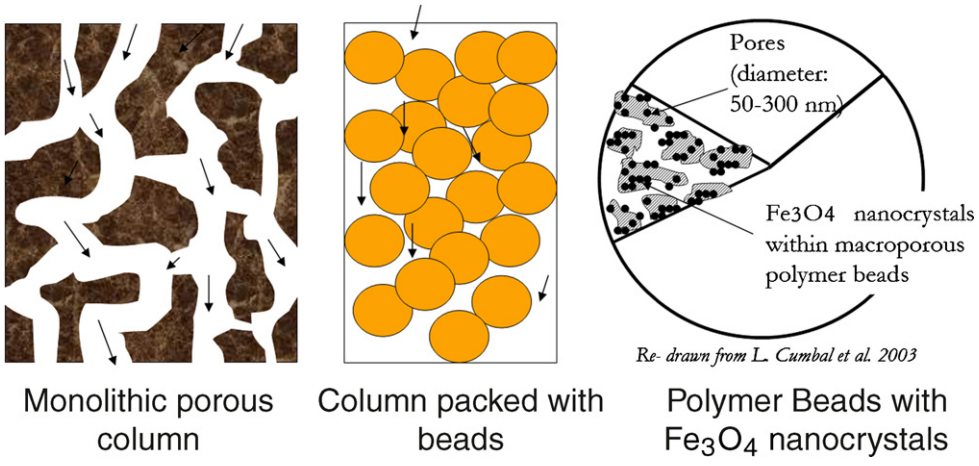

Fig. 2. The water flow in devices based on monolithic porous gels and polymer beads.
Adapted from: Cumbal et al. [29].

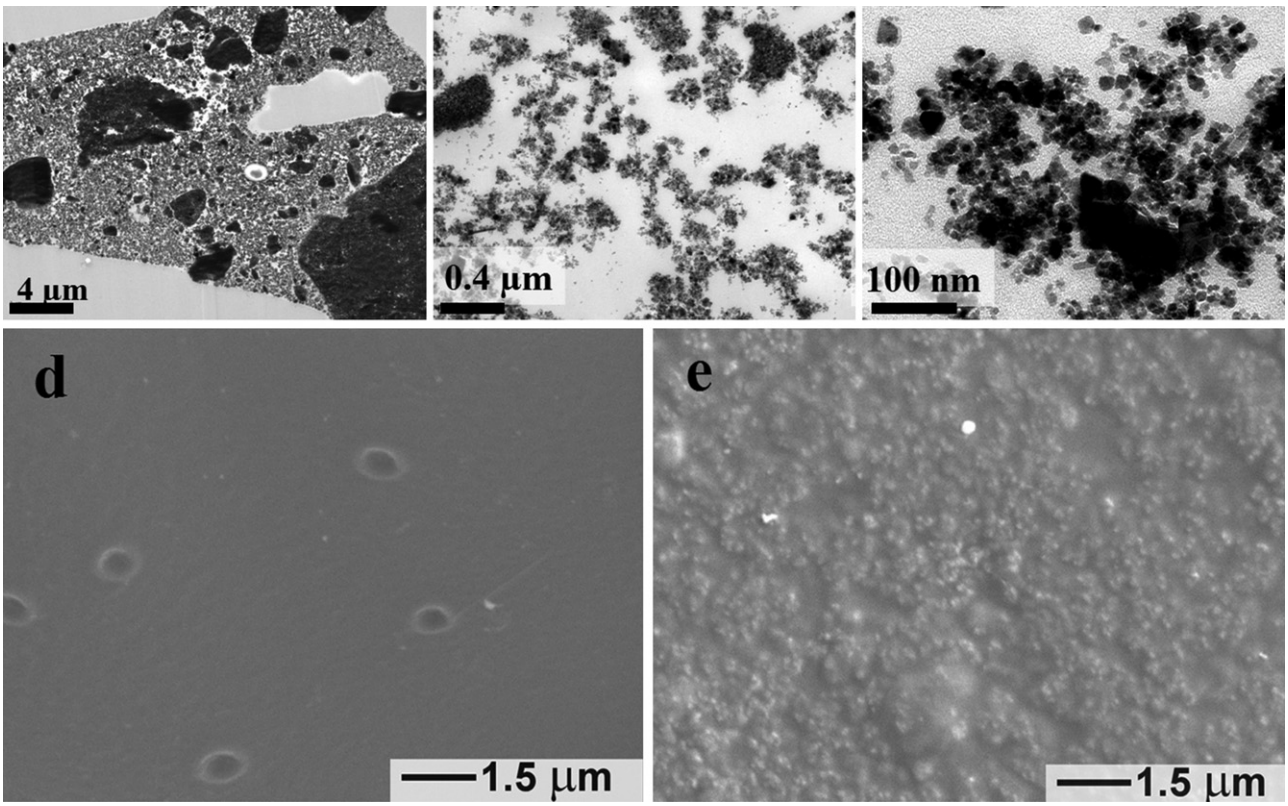

Fig. 3. TEM images of a transverse section through a Fe_3O_4–MG with the iron oxide nanoparticles randomly distributed inside the polymer wall (a–c). High magnification TEM image reveals agglomerated nanoparticles. (d) SEM image of the HEMA gel polymer wall surface without particles and (e) SEM image of composite polymer wall surface showing a relatively even distribution of iron oxide nanoparticles and nanoparticle agglomerates across the surface. Gels were prepared at −12 °C.

tem. The ice crystals serve as a pore forming substance in these systems. The materials have been shown previously to have very good adsorption performance in a number of bioseparation applications, including the treatment of complex solutes without the requirement for additional purification steps [22,24]. Monolithic columns with anion-exchange or affinity groups have been used for direct capture of proteins, antibodies or whole cells by applying non-purified cell lysate or cell suspension onto the column (particle size 1–10 μm) [25–27]. Because of the presence of large interconnected pores a particulate solution could be easily pumped through the monolithic gels without column clogging or blocking the flow. As such, these macroporous gels provide a high flow-through capability and a potentially stable scaffold for iron-nanoparticles.

3.2. Macroporous iron nanoparticle–polymer monolith production and characteristics

Macroporous gels (MG) with embedded α-Fe_2O_3 or Fe_3O_4 nanoparticles (α-Fe_2O_3–MGs and Fe_3O_4–MGs, respectively) were prepared by polymerization of HEMA and PEGDA monomers in suspension with iron oxide nanoparticles. On freezing, iron nanoparticles were expelled by ice crystals together with the monomer and cross-linker and after polymerization a macroporous polymer network with embedded iron oxide particles formed. The composite gels have large interconnected pores of up to 100 μm diameter (Fig. 1).

All α-Fe_2O_3–MGs and Fe_3O_4–MGs produced have a macroporous structure with interconnected pores (Fig. 1), which provides a low resistance to water flow through the gel. The flow rate measured at constant hydrostatic pressure of ~0.01 MPa was 2.29 ± 0.34 and 2.78 ± 0.33 ($\times 10^{-3}$) m s^{-1} for the α-Fe_2O_3–MGs and Fe_3O_4–MGs packed in the glass column, respectively (Table 1). Composite gels have similar flow rates to the gel prepared without nanoparticles (Table 1), thus addition of nanoparticles has a negligible effect on the flow resistance of the composite gel monoliths.

The 3D structure of the large interconnected pores directs the flow of water in a way that contaminants dissolved in the water pass in direct contact with the nanoparticle impregnated polymer surface (Fig. 2). In a device packed with beads (300–1200 μm in diameter [17,28]), where iron nanoparticles are embedded in the pore structure of the beads, the water must flow through the channels between the beads generating a high back-flow resistance and then diffuse into the iron nanoparticle containing channels (50–300 nm; Fig. 2). For instance ArsenX is a commercially available resin with iron particles and has a recommended flow rate of 5.0×10^{-5} to 1.1×10^{-4} m s^{-1} (20–40 bed volumes/h) at conventional pressures up to 0.8 MPa [17,28]. The rate of adsorption in such structures is likely to be slow and diffusion limited. The unique structure of the large interconnected pores and low flow resistance of the macroporous gels provides a higher flow rate at relatively low pressures, rendering a device for rapid and effective treatment of contaminated water.

Scanning and transmission electron micrographs show that the nanoparticles and nanoparticle agglomerates embedded inside the polymer matrix are relatively evenly distributed within the polymer wall (Fig. 3). The iron oxide content in the gels determined by extraction with 2 M HCl and TGA was found to be 0.059–0.077 and 0.078–0.095 g/g hydrated gel, for α-Fe_2O_3–MG and Fe_3O_4–MG, respectively (Table 1).

Because of their higher density, iron oxide nanoparticles sediment during the composite gel preparation resulting in a gradient distribution of particles along the column. The concentration of iron in the composites measured by TGA, was lower at the top of the monolithic nanocomposite (0.35 g/g of dried gel) and higher at the bottom (0.59 g/g of dried gel). A gradient free adsorption column could be generated using smaller pieces (discs) of the composite

Table 2
Mechanical properties of composite gel. Gels were prepared at −18 °C.

Gels	Compression modulus (kPa)	Stiffness (kPa)
HEMA–MGs	4.4 ± 0.9	16.4 ± 1.9
α-Fe_2O_3–MGs	4.6 ± 1.3	46.8 ± 4.9
Fe_3O_4–MGs	6.0 ± 1.0	57.6 ± 10.8

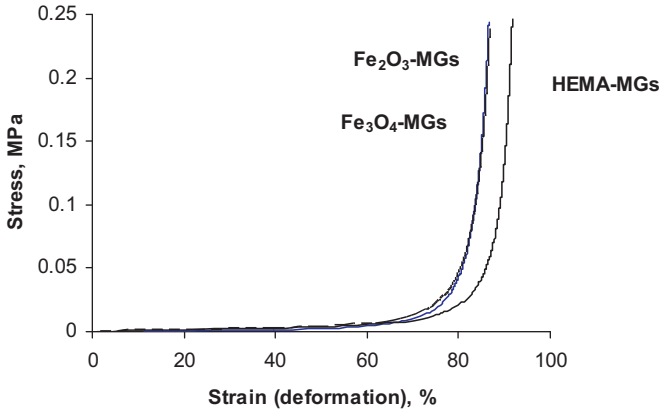

Fig. 4. Stress-strain curves for HEMA gel and composites incorporating α-Fe_2O_3 and Fe_3O_4. Gels were prepared at −18 °C.

gels which have a non-significant gradient distribution of iron oxide particles.

3.3. Mechanical properties

The compression modulus of the composite gels was in the range 4.4–6.0 kPa, similar to gels without iron oxide particles (Table 2). The stress–strain curve showed the typical behaviour for highly elastic materials with extensive flexibility and shape recovery properties against compression (Fig. 4). The composite gels were compressed up to 85% at maximal loading (18 N) without rupture. Embedding the iron oxide particles inside the gel matrix has no discernible effect on their compression modulus; however the nanoparticle composites were stiffer than gels without nanoparticles as a result of embedding nanoparticles inside the polymer matrix. The stiffness of the composite gels (estimated as the stress required to achieve 80% deformation) was 46.8 ± 4.9 kPa and 57.6 ± 10.8 kPa for α-Fe_2O_3 and Fe_3O_4 composites, respectively, compared with 16.4 ± 1.9 kPa for a HEMA-only gel.

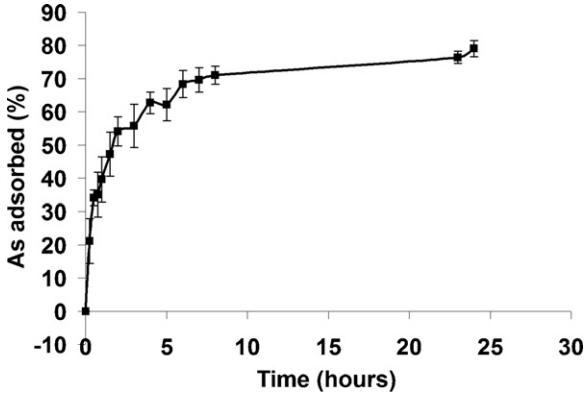

Fig. 5. Adsorption kinetics of As(III) onto Fe_3O_4–MG. Composite gel weight was 0.5 g, solution volume 500 ml, initial As(III) concentration in initial solution was 2 mg/l. Gels were prepared at −12 °C.

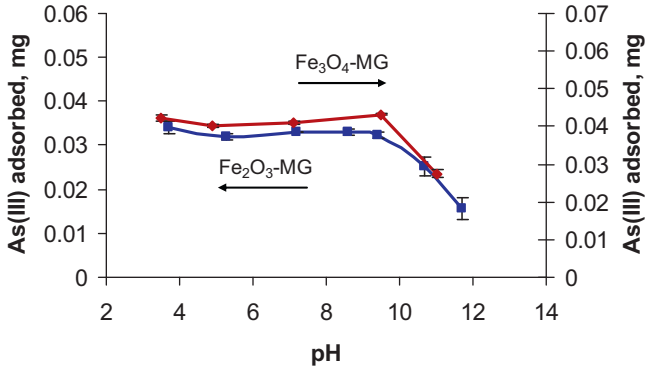

Fig. 6. Adsorption of As(III) by α-Fe_2O_3–MGs and Fe_3O_4–MGs at different pH. The composite gel weight was 0.5 g, solution volume 10 ml, shaking time 1.5 h for Fe_3O_4–MGs and 3 h for α-Fe_2O_3–MGs, initial arsenic concentration 4 mg/l. Error bars are smaller than the marker symbols used on the plot unless shown otherwise.

3.4. Adsorption of As(III)

The composite gels were tested for adsorption of As(III) from aqueous solution. Numerous previous studies have highlighted the high sorption capacity of iron oxides towards arsenite and arsenate [3,17,29,30]. However, it was anticipated that the embedding of nanoparticles inside a polymer matrix would reduce their accessibility for interaction with the target contaminant and so inhibit their adsorptive properties. The adsorption of arsenic by iron oxide nanoparticles embedded in the macroporous gel was therefore studied in comparison with adsorption onto free iron oxide nanoparticles (i.e. as supplied by the Arry International Group Ltd. in the form of 20–30 nm particle size). Approximately a three-fold reduction in adsorption capacity was observed for the α-Fe_2O_3 and Fe_3O_4 composite material compared to the free nanoparticles. The equilibrium adsorption capacity of As(III) for the α-Fe_2O_3–MGs and Fe_3O_4–MGs was 0.21 and 0.23 As(III) mg/ml of gel or 2.7 and 3.1 mg of arsenic per gram of nanoparticles, respectively, while free nanoparticles adsorbed about 9 mg of As(III) per gram of nanoparticles (Table 3). Thus, while embedding of nanoparticles inside the polymer matrix does reduce arsenic adsorption, the iron oxide nanoparticles still retain significant reactivity following immobilization. Analysis of As speciation indicates a dominance of As(III)

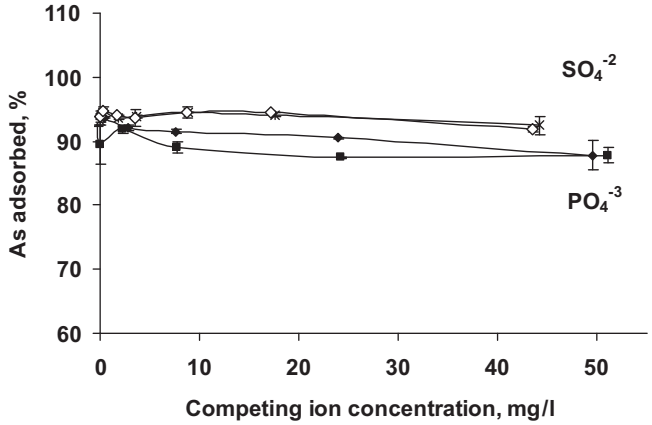

Fig. 7. Effect of PO_4^{3-} and SO_4^{2-} on As(III) adsorption for α-Fe_2O_3 and Fe_3O_4 composite gel. Closed squares and closed diamonds profiles show effect of PO_4^{3-} on As(III) adsorption for α-Fe_2O_3 and Fe_3O_4 composite gel, respectively, star and open diamond profiles show effect of SO_4^{2-} on As(III) adsorption for α-Fe_2O_3 and Fe_3O_4 composite gel. The composite gel weight was 0.4 g, solution volume 20 ml, shaking time 20 h, As(III) concentration = 5 mg/l, pH 7.0. Error bars are smaller than the marker symbols used, unless shown otherwise.

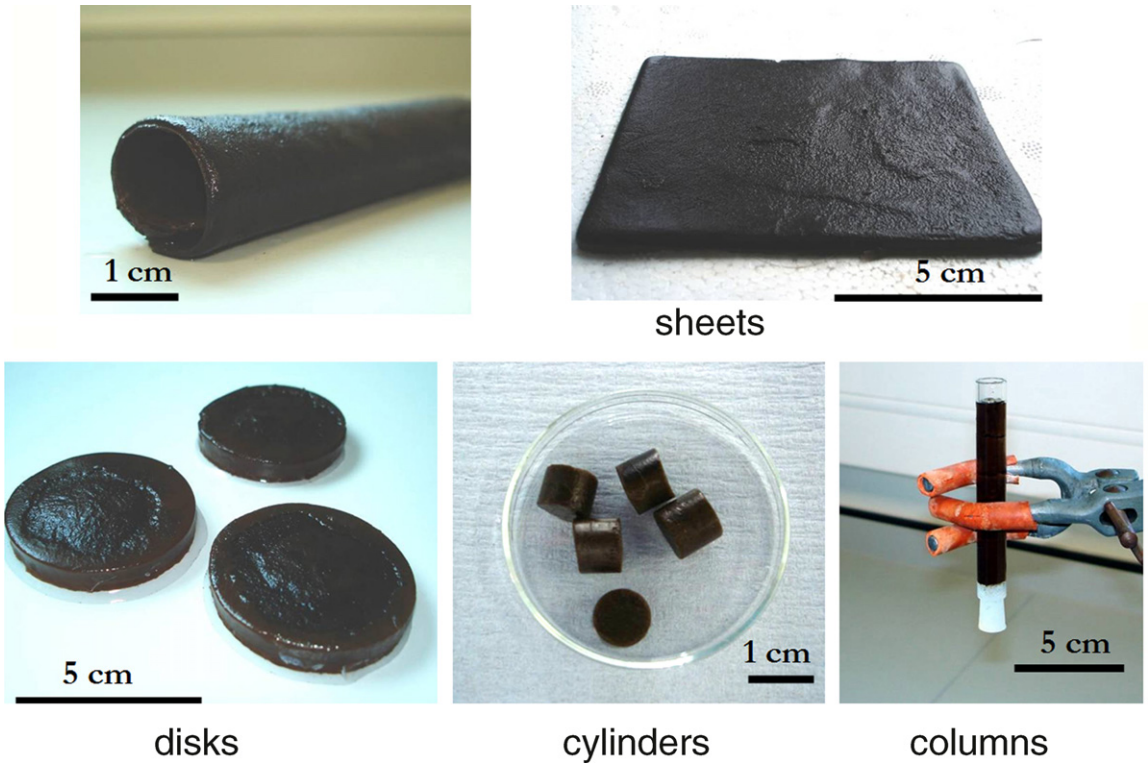

Fig. 8. Macroporous gel Fe nanoparticle composites in different configurations.

species (98%) in the solutions demonstrating the efficiency of the composite material for removing As(III).

It was demonstrated by Giménez et al. [31] that As(III) adsorption on natural hematite was more efficient than on goethite and magnetite. In our study, we have found a similar relationship. Both α-Fe_2O_3 and Fe_3O_4 have similar adsorption capacity per milligram of nanoparticles (Table 3). However, the Fe_3O_4 particles are smaller in size and have a larger surface area (60 m^2/g) available for adsorption compared to α-Fe_2O_3 (50 m^2/g). Thus the adsorption capacity of α-Fe_2O_3 calculated per unit surface area is higher (0.18 mg/m^2) compared to Fe_3O_4 (0.16 mg/m^2). In the composite, we see the same tendency.

Studies of adsorption kinetics show a rapid decrease of As(III) concentration in the solution in the first hour with a slower rate of adsorption subsequently (Fig. 5). About 70% of As(III) was adsorbed from 2 mg/l As(III) solution within the first 5 h (Fig. 5). The decrease of As(III) adsorption after the first 5 h is likely a result of less accessibility of nanoparticles embedded in deeper polymer layers and the longer time required for As(III) diffusion into the polymer.

The iron concentration in the solution after adsorption was found to be negligible in all experiments, indicating that the particles were stably embedded inside the polymer matrix and were not released into solution.

Arsenic removal by the α-Fe_2O_3 and Fe_3O_4 composites was largely unaffected by pH across a pH range of 3 – 9 (Fig. 6), though a small decrease in As(III) adsorption was observed at higher pH (>10, Fig. 6). The pH of solution controls the speciation of arsenic and the surface charge of the iron oxide. At more alkaline pH, anionic species of As(III) will dominate [32] and the surface of the iron oxide will also be negatively charged causing the electrostatic repulsion of anionic species [31]. Similar results have been reported in other studies, where a decrease of As(III) adsorption on magnetite at pH > 9 was observed [31,33].

In addition to pH effects, the adsorption efficiency will also be influenced by the presence of other chemical species [34,35]. Commonly, arsenic adsorption is decreased in the presence of phosphate because of competition for the binding sites of the adsorbent between arsenic and phosphate ions [34,36]. The influence of competing ions, such as phosphate and sulphate, on As(III) removal was studied by adding different amounts of PO_4^{3-} and SO_4^{2-} to the arsenic solution. Adsorption of As(III) by α-Fe_2O_3 and Fe_3O_4 composites was unaffected by the presence of SO_4^{2-} (Fig. 7) even at high SO_4^{2-} concentrations of 45 mg/l. A slight reduction in adsorption capacity (of about 10%) was detected with increasing PO_4^{3-} concentration (Fig. 7).

Table 3
Equilibrium adsorption capacity of materials for As(III).

Samples	As(III) mg/g of Fe particles	As(III) mg/ml of gel
α-Fe_2O_3, free nanoparticles	9.0 ± 1.6	NA
Fe_3O_4, free nanoparticles	9.6 ± 2.4	NA
HEMA–MGs	NA	0.008
α-Fe_2O_3–MGs	3.1 ± 0.40	0.21 ± 0.03
Fe_3O_4–MGs	2.7 ± 0.21	0.23 ± 0.02

3.5. Potential configuration/implementation for water clean-up

Use of macroporous gels as a substrate or scaffold for Fe nanoparticles allows generation of reactive nanocomposite devises which can be produced in variety of end-use configurations: monolithic blocks, polymer sheets, discs or columns for through-flow (or flow-over) applications (Fig. 8). Alternatively, gel-based composites may be manufactured within robust plastic carriers (e.g. [37]) for more aggressive physical settings (e.g. in settlement tanks, fluidised beds, etc.) which provides significant flexibility in terms of device configuration. Additionally the macroporous polymer could be modified to enhance removal of other target compounds with ion-exchange groups [38–40] or through molecular imprinting of the polymer [37,41].

4. Conclusions

The composite gels prepared by the cryopolymerisation technique have a unique structure of interconnected large pores, with mechanical stability and low flow resistance that (together with the flexibility of producing these materials in a range of configurations) make them excellent materials for use as a support for nanoparticles in developing absorption/filtration devices for the clean-up of ground water, surface waters and drinking water. α-Fe_2O_3 and Fe_3O_4 nanoparticles were physically embedded within the macroporous polymer gel preventing their release into the environment while maintaining their reactivity. The macroporous polymer gels with embedded iron oxide nanoparticles were effective in removing of As(III) from aqueous solution over a wide pH range and were largely unaffected by the presence of competing ions, such as sulphate and phosphate.

Acknowledgement

This work was financially supported by FP7 project PIEF-GA-2008-220212-MACRO-CLEAN. We thank Alina Korobeinyk (University of Brighton) for assistance with TGA, and Dr Julian Thorpe (Sussex University) for TEM sample preparation. Dr. R. Whitby thanks the Research Council United Kingdom Academic Fellowship programme. The authors are grateful to Protista Biotechnology AB (www.protista.se) for access to monolithic porous polymer structure (MPPS®) materials and technologies.

References

[1] W.X. Zhang, Nanoscale iron particles for environmental remediation: an overview, J. Nanopart. Res. 5 (2003) 323–332.
[2] C.B. Wang, W.X. Zhang, Synthesizing nanoscale iron particles for rapid and complete dechlorination of TCE and PCBs, Environ. Sci. Technol. 31 (1997) 2154–2156.
[3] J.T. Mayo, C. Yavuz, S. Yean, L. Cong, H. Shipley, W. Yu, J. Falkner, A. Kan, M. Tomson, V.L. Colvin, The effect of nanocrystalline magnetite size on arsenic removal, Sci. Technol. Adv. Mater. 8 (2007) 71–75.
[4] USEPA, Nanotechnology White Paper. ERA 100/B-07/001, Science Policy Council, U.S. Environmental Protection Agency, Washington, DC, 2007, p. 120.
[5] Y.P. Sun, X.Q. Li, J. Cao, W.X. Zhang, H.P. Wang, Characterization of zero-valent iron nanoparticles, Adv. Colloid Interface Sci. 120 (2006) 47–56.
[6] A.B. Cundy, L. Hopkinson, R.L.D. Whitby, Use of iron-based technologies in contaminated land and groundwater remediation: a review, Sci. Total Environ. 400 (2008) 42–51.
[7] V.L. Colvin, The potential environmental impact of engineered nanomaterials, Nat. Biotechnol. 21 (2003) 1166–1170.
[8] R.D. Handy, R. Owen, E. Valsami-Jones, The ecotoxicology of nanoparticles and nanomaterials: current status, knowledge gaps, challenges, and future needs, Ecotoxicology 17 (2008) 315–325.
[9] A.B Boxall, K. Tiede, Q. Chaudhry, Engineered nanomaterials in soils and water: how do they behave and could they pose a risk to human health, Nanomedicine 2 (2007) 919–927.
[10] M.N. Moore, Do nanoparticles present ecotoxicological risks for the health of the aquatic environment, Environ. Int. 32 (2006) 967–976.
[11] M.R. Wiesner, G.V. Lowry, P. Alvarez, D. Dionysiou, P. Biswas, Assessing the risks of manufactured nanomaterials, Environ. Sci. Technol. 40 (2006) 4336–4345.
[12] M. Valko, H. Morris, M.T. Cronin, Metals, toxicity and oxidative stress, Curr. Med. Chem. 12 (2005) 1161–1208.
[13] B. Nowack, T.D. Bucheli, Occurrence, behavior and effects of nanoparticles in the environment, Environ. Pollut. 150 (2007) 5–22.
[14] M. DeMarco, A. SenGupta, J.E. Greenleaf, Arsenic removal using a polymeric/inorganic hybrid sorbent, Water Res. 37 (2003) 164–176.
[15] O.M. Vatutsina, V.S. Soldatov, V.I. Sokolova, J. Johann, M. Bissen, A. Weissenbacher, A new hybrid (polymer/inorganic) fibrous sorbent for arsenic removal from drinking water, React. Funct. Polym. 67 (2007) 184–201.
[16] J.E. Greenleaf, J.C. Lin, A.K. SenGupta, Two novel applications of ion exchange fibers: arsenic removal and chemical-free softening of hard water, Environ. Prog. 25 (2006) 300–311.
[17] P. Sylvester, P. Westerhoff, T. Möller, M. Badruzzaman, O. Boyd, A hybrid sorbent utilizing nanoparticles of hydrous iron oxide for arsenic removal from drinking water, Environ. Eng. Sci. 24 (2007) 104–112.
[18] F.M. Plieva, I.N. Savina, S. Deraz, J. Andersson, I.Y. Galaev, B. Mattiasson, Characterization of supermacroporous monolithic polyacrylamide based matrices designed for chromatography of bioparticles, J. Chromatogr. B 807 (2004) 129–137.
[19] X.C. Le, S. Yalcin, M. Ma, Speciation of submicrogram per liter levels of arsenic in water: on-site species separation integrated with sample collection, Environ. Sci. Technol. 34 (2000) 2342–2347.
[20] I.N. Savina, V. Cnudde, S. D'Hollander, L. Van Hoorebeke, B. Mattiasson, I.Y. Galaev, F. Du Prez, Cryogels from poly(2-hydroxyethyl methacrylate): macroporous, interconnected materials with potential as cell scaffolds, Soft Mater. 3 (2007) 1176–1184.
[21] I.N. Savina, P.E. Tomlins, S.V. Mikhalovsky, I.Y. Galaev, Porosity characterization, in: B. Mattiasson, A. Kumar, I.Y. Galaev (Eds.), Macroporous Polymers: Production, Properties and Biotechnological/Biomedical Applications, Taylor and Francis, 2009, pp. 211–235.
[22] V.I. Lozinsky, I.Y. Galaev, F.M. Plieva, I.N. Savina, H. Jungvid, B. Mattiasson, Polymeric cryogels as promising materials of biotechnological interest, Trends Biotechnol. 21 (2003) 445–451.
[23] V.I. Lozinsky, Cryogels on the basis of natural and synthetic polymers: preparation, properties and application, Russ. Chem. Rev. 71 (2002) 489–511.
[24] F.M. Plieva, I.Y. Galaev, B. Mattiasson, Monolithic gels prepared at subzero temperatures as novel materials for chromatography of particulate-containing fluids and cell culture applications, J. Sep. Sci. 30 (2007) 1657–1671.
[25] A. Hanora, I. Savina, F.M. Plieva, V.A. Izumrudov, B. Mattiasson, I.Y. Galaev, Direct capture of plasmid DNA from non-clarified bacterial lysate using polycation-grafted monoliths, J. Biotechnol. 123 (2006) 343–355.
[26] M.B. Dainiak, I.Y. Galaev, A. Kumar, F.M. Plieva, B. Mattiasson, Chromatography of living cells using supermacroporous hydogels, cryogels, Adv. Biochem. Eng./Biotechnol. (2007) 1–18.
[27] P. Persson, O. Baybak, F.M. Plieva, I.Y. Galaev, B. Mattiasson, B. Nilsson, A. Axelsson, Characterization of a continuous supermacroporous monolithic matrix for chromatographic separation of large bioparticles, Biotechnol. Bioeng. 88 (2004) 224–236.
[28] ArsenX, http://www.systematixusa.com/products/media/active_media/arsenx.htm (Product data, accessed on 26.01.11).
[29] L. Cumbal, J. Greenleaf, D. Leun, A.K. SenGupta, Polymer supported inorganic nanoparticles: characterization and environmental applications, React. Funct. Polym. 54 (2003) 167–180.
[30] D. Mohan, J.C.U. Pittman, Arsenic removal from water/wastewater using adsorbents—a critical review, J. Hazard. Mater. 142 (2007) 1–53.
[31] J. Giménez, M. Martínez, J. De Pablo, M. Rovira, L. Duro, Arsenic sorption onto natural hematite, magnetite, and goethite, J. Hazard. Mater. 141 (2007) 575–580.
[32] P.L. Smedley, D.G. Kinniburgh, A review of the source, behaviour and distribution of arsenic in natural waters, Appl. Geochem. 17 (2002) 517–568.
[33] C. Su, R.W. Puls, Arsenate and arsenite sorption on magnetite: relations to groundwater arsenic treatment using zerovalent iron and natural attenuation, Water Air Soil Pollut. 193 (2008) 65–78.
[34] M. Stachowicz, T. Heimstra, W.H. van Riemsdijk, Multi-competitive interaction of As(III) and As(V) oxyanions with Ca^{2+}, Mg^{2+}, PO_4^{3-}, and CO_3^{2-} ions on goethite, J. Colloid Interface Sci. 320 (2008) 400–414.
[35] M. Stachowicz, T. Heimstra, H. Willem, Arsenic–bicarbonate interaction on goethite particles, Environ. Sci. Technol. 41 (2007) 5620–5625.
[36] W. Shao, X. Li, Q. Cao, F. Luo, J. Li, Y. Du, Adsorption of arsenate and arsenite anions from aqueous medium by using metal(III)-loaded amberlite resins, Hydrometallurgy 91 (2008) 138–143.
[37] M. Le Noir, F. Plieva, B. Mattiasson, Removal of endocrine-disrupting compounds from water using macroporous molecularly imprinted cryogels in moving-bed reactor, J. Sep. Sci. 32 (2009) 1471–1479.
[38] I.N. Savina, I.Y. Galaev, B. Mattiasson, Ion-exchange macroporous hydrophilic gel monolith with grafted polymer brushes, J. Mol. Recognit. 19 (2006) 313–321.
[39] I.N. Savina, I.Y. Galaev, B. Mattiasson, Anion-exchange supermacroporous monolithic matrices with grafted polymer brushes of N,N-dimethylaminoethyl-methacrylate, J. Chromatogr. A 1092 (2005) 199–205.
[40] I.N. Savina, B. Mattiasson, I.Y. Galaev, Graft polymerization of acrylic acid onto macroporous polyacrylamide gel (cryogel) initiated by potassium diperiodatocuprate, Polymer 46 (2005) 9596–9603.
[41] M. Le Noir, F. Plieva, T. Hey, B. Guieysse, B. Mattiasson, Macroporous molecularly imprinted polymer/cryogel composite systems for the removal of endocrine disrupting trace contaminants, J. Chromatogr. A 1154 (2007) 158–164.